Core-Shell Interface Oriented Synthesis of Bowl-Structured Hollow Silica Nanospheres Using Self-Assembled ABC Triblock Copolymeric Micelles

Md Nuruzzaman[ab], Yanju Liu[ab], Mohammad Mahmudur Rahman[ab], Ravi Naidu[ab], Rajarathnam Dharmarajan[ab], Ho Kyong Shon[bc], and Yun Chul Woo[d]*

[a]Global Centre for Environmental Remediation (GCER), Faculty of Science, The University of Newcastle, University Drive, Callaghan, NSW 2308, Australia

[b]Cooperative Research Centre for Contamination Assessment and Remediation of the Environment (CRC CARE), ATC Building, The University of Newcastle, Callaghan, NSW 2308, Australia

[c]Centre for Technology in Water and Wastewater, School of Civil and Environmental Engineering, University of Technology Sydney (UTS), P.O. Box 123, 15 Broadway, NSW 2007, Australia

[d]Environment and Plant Research Institute, Korea Institute of Civil Engineering and Building Technology (KICT), 283, Goyangdae-Ro, Ilsanseo-Gu, Goyang-Si, Gyeonggi-Do 411-712, Republic of Korea

*Corresponding author: Ravi Naidu,

Email: Ravi.Naidu@newcastle.edu.au; Ravi.Naidu@crccare.com

Postal address: Room 147, ATC Building, The University of Newcastle, University Drive, Callaghan, NSW 2308, Australia

Core-Shell Interface Oriented Synthesis of Bowl-Structured Hollow Silica Nanospheres Using Self-Assembled ABC Triblock Copolymeric Micelles

Md Nuruzzaman[ab], Yanju Liu[ab], Mohammad Mahmudur Rahman[ab], Ravi Naidu[ab], Ho Kyong Shon[bc], Rajarathnam Dharmarajan[ab], and Yun Chul Woo[c]*

ABSTRACT

Hollow porous silica nanospheres (HSNs) are emerging classes of cutting-edge nanostructured materials. They have elicited much interest as carriers of active molecules delivery due to their amorphous chemical structure, non-toxic nature and biocompatibility. Structural development with hierarchical morphology is mostly required for obtaining the desired performance. In this context, large through-holes or pore openings on shells are desired so that the post-synthesis loading of active molecules HSNs via a simple immersion method can be facilitated. This study reports the synthesis of HSNs with large through-holes or pore openings on shells, which are subsequently termed bowl-structured hollow porous silica nanospheres (BHSNs). The synthesis of BHSNs was mediated by the core-shell interfaces of the core-shell-corona structured micelles obtained from a commercially available ABC triblock copolymer (polystyrene-b-poly(2-vinyl pyridine)-b-poly(ethylene oxide) (PS-P2VP- PEO)). In this synthesis process, polymer@SiO_2 composite structure was formed because of the deposition of silica (SiO_2) on the micelles' core. The P2VP block played the significant role in: firstly, hydrolysis and condensation of the silica precursor i.e. tetraethylorthosilicate (TEOS); and secondly, maintaining the shell's growth. The

PS core of the micelles built the void spaces. Transmission electron microscopy (TEM) images revealed a spherical hollow structure with an average particle size of 41.87 ± 3.28 nm. The average diameter of void spaces was 21.71 ± 1.22 nm and shell thickness was 10.17 ± 1.68 nm. According to the TEM image analysis the average large pore was determined as 15.95 nm. Scanning electron microscopy (SEM) images further confirmed the presence of large single pores or openings in shells. These were formed due to the accumulated ethanol on PS core acting to prevent the growth of silica.

KEYWORDS. Silica nanospheres, Bowl-structure, Interfacial synthesis, ABC triblock copolymer, Hollow structure.

INTRODUCTION

Inorganic hollow-structured nanomaterials have emerged as potentially useful functional phenomena. Such nanomaterials have generated increasing research interest as carriers of active molecules, because they have potential in helping develop controlled delivery systems in various fields. This is due to their large specific surface area, low density, mechanical and thermal stabilities, surface permeability, high loading capacity, controllable structure, and a wide range of applications.[1-3] Among the various hollow-structured inorganic nano-carriers, silica-based nanoparticles such as hollow porous silica nanospheres (HSNs) are considered most promising because of their amorphous chemical structure, non-toxic nature[4] and biocompatibility[5]. As well as drug delivery their potential applications have been extended to agrochemical delivery, especially pesticides, particularly over the last decade.[6-9] It is expected that such carrier materials

77 can be utilized for the preparation of controlled-release formulations (CRFs) due to the novel
78 properties of nano-size particles or materials.[10]

79 It is important to ensure the quality and uniform particle size of nanospheres during their
80 synthesis so that the desired performance will be obtained.[11] Recent studies suggest that the size
81 of pores in the shells of hollow nanosphere material is important because they play a significant
82 role in the encapsulation and delivery of functional substances.[12] For example, HSNs' performance
83 declines during post-synthesis loading by simple immersion methods because of small mesopores
84 (2-5 nm).[8,9] Loading active molecules after synthesis mainly depends on diffusion processes and
85 the efficiency of this loading varies according to the size of mesopores in the shell. Therefore,
86 technology such as high-pressure supercritical fluid loading is required to facilitate post-synthesis
87 loading of active molecules into the inner core or void space of HSNs.[8,9] More importantly, to
88 serve as an ideal carrier, the HSNs must be structured with an appropriate pore size that is larger
89 than the kinetic diameter of the respective active molecules.[13,14] It was reported that pore size less
90 than 10 nm often obstructs the application of ordered mesoporous nanomaterials in many fields
91 especially where it requires a fast transport and efficient loading of large-size active molecules
92 such as genetic material, proteins, drugs, organic bioactive molecules etc.[15]

93 In this aspect, hollow nanospheres or microspheres with large through-holes (HMLS), or pore
94 openings wider than 10 nm, are highly desirable for facilitating the loading of active guest
95 molecules.[16] HMLS can even encapsulate large molecules, for example proteins or DNA[17], with
96 diffusion this processes producing any limitations. The guest molecules could also be delivered in
97 a controlled way from such nanocarriers where initially a fast release rate is observed which is
98 desired in many applications such as drug delivery, pesticide delivery etc. to compensate rapidly
99 against the target germs or pests. Later on, a sustained releasing profile is observed due to

electrostatic interaction and/or hydrogen bonding interaction between the guest molecules and Si-OH groups of HMLs.[18] However, to accomplish sustained release profile surface functionalization seems to be essential where large through-holes facilitate the surface functionalization process to modify the inner core surfaces on demand. In this case, with increasing amounts of surface functionalization agents may reduce the loading capacity but slow releasing profile is observed. In addition, the guest molecules also could be delivered to the target more efficiently preparing environmentally responsive controlled release system through post loading surface functionalization or coating with polymers.[18-20]

To date, various synthetic methods for producing hollow microspheres with a large shell pore size (>10 nm) have utilized approaches such as template-directed synthesis, shell-breaking, Ostwald ripening and galvanic replacement reaction.[16] These methods have produced various kinds of HMLS with single, multiple and hierarchal shell holes, and depending on their morphology, the spheres have been termed bowl-like[21,22], mouth-like[23], golf ball-like[24], or cage-like[25]. It is apparent that the physico-chemical properties of synthesized hollow-structured nanomaterials vary depending on their synthesis technique. Several methods have been employed for synthesizing HSNs, such as sacrificial hard templates, polymeric soft templates, surfactant/vesicle templates and emulsion templating technique, producing various shell thicknesses and porosity of structures.[5,26] Among these methods, hard templating method suffers from certain limitations. In the hard templating approach, removing the template is complicated, time-consuming and unsuitable for mass production due to the utilization of costly hard template.[27,28] While the soft templating approach offers more opportunities for large scale synthesis of mesoporous materials compared to hard templating approach.[29] Of the various soft templates based on cationic surfactants or Pluronic amphiphilic block copolymers were employed

initially for the synthesis of mesoporous nanomaterials.[15] However, they can produce only a small pore size due to their short chain length.[27] Thus, non-Pluronic based amphiphilic AB diblock or symmetric ABA triblock copolymers consisting of hydrophilic segments, such as PEO, poly(L-glutamic acid) (PLGA), poly(2-vinylpyridine) (P2VP) or poly(4-vinylpyridine) (P4VP), and hydrophobic segments such as polystyrene (PS), polyisoprene (PI), polybutadiene (PB) and polyacrylonitrile (PAN) created much attention for synthesizing various mesoporous materials.[27,28] With such block copolymers the mesoporous structure, shape, pore size is also considered to be adjustable by controlling the synthesis conditions (such as temperature, pH, ionic strength etc.) and properties of the block copolymers (such as composition, block sequence, molecular weights, volume fractions etc.).[14,29,30] Along with block copolymer, various amphiphilic polypeptides are also utilized for the synthesis of mesoporous materials through biomineralization process.[31-34] Nonetheless, aggregation of nanoparticles is a common phenomenon observed in these processes.[35] Generally, non-Pluronic and polypeptide based amphiphilic AB diblock or symmetric ABA triblock copolymers were found mostly suited for synthesizing 2-D or 3-D structured mesoporous materials. Synthesis of zero dimensional nanomaterial is still challenging utilizing such block copolymers. Therefore, HSNs with large through-holes with several morphologies that have been synthesized using these templates were not uniform, even when the particle size was observed larger than 100 nm.

Advances in interfacial chemistry have enabled HSNs synthesis by more effectively controlling the nucleation and growth of silica on templates. Recent studies have shown that ABC triblock copolymers are able to form micelles with a core-shell-corona structure due to their self-assembling properties. This capacity makes them excellent templates for synthesizing several uniform and monodispersed hollow porous nanomaterials including HSNs.[11,35-38] For example,

146 micelles of poly(styrene-*b*-2-vinyl pyridine-*b*-ethylene oxide) (PS-P2VP-PEO) were successfully
147 utilized for the synthesis of HSNs where tetramethyl orthosilicate was used as a silica
148 precursor.[11,35,36] Nonetheless, no large pore was observed in the shell of HSNs during this synthesis
149 process.

150 It is well investigated that each chemical involved in the synthesis of HSNs can play a significant
151 role in their morphology and behavior. It is expected that changing the precursor to
152 tetraethylorthosilicate (TEOS) instead of tetramethylorthosilicate (TMOS) for the synthesis of
153 HSNs using core-shell-corona structured micelles of PS-P2VP-PEO triblock copolymer utilized
154 as soft template will facilitate the production of large through-holes or pore openings in the shell
155 of HSNs. Generally, TMOS and TEOS are the most widely used precursors for the synthesis of
156 silica using the sol-gel process.[39] During the hydrolysis of these precursors, TEOS generates more
157 hydrophobic by-products such as ethanol (logP= -0.18) compared to methanol (logP= -0.69),
158 which is the by-product of hydrolyzed TMOS. In contrast the hydrolysis and condensation rate of
159 TMOS is faster than that of TEOS.[40] Thus, it is expected that during the hydrolysis process the
160 ethanol will be able to interact with the hydrophobic PS block more efficiently. Accumulation of
161 ethanol as droplets will be further promoted by hydrogen bonding interaction with the P2VP block.
162 Consequently, deposition of silica will be prevented and as a result, large through-holes or pores
163 in the shell of HSNs will be observed after calcination.

164 Considering the hypothetical mechanisms, this study was conducted to synthesize HSNs with
165 large through holes or pore openings in shells termed as bowl-structured hollow porous silica
166 nanospheres (BHSNs) using the core-shell interfacial chemistries of the micelles. This study
167 presents a detailed synthesis process concerning BHSNs. Specifically, we determined the effects
168 of changing the precursor to TEOS instead of TMOS on particle morphology while the triblock

copolymer micelles of PS-P2VP-PEO with a core-shell-corona structure serve as a soft template. This study also presents plausible mechanisms for the synthesis of BHSNs and investigates the characteristics of synthesized BHSNs to establish their potential for future applications.

EXPERIMENTAL SECTION

Materials and reagents

PS-P2VP-PEO triblock copolymer with block sizes PS(20k)–P2VP(15k)–PEO(27k) was purchased from Polymer Source Inc., Canada. The number in parentheses represents the average molar mass (Mn) of the block chains, e.g., 20k denotes 20,000 g mol^{-1}. The poly-dispersity index (PDI), or ratio of weight average molecular weight (Mw) and number average molecular weight (Mn) of the tri-block copolymer, was 1.11. The chemical structure of the block copolymer is presented in Supporting Information (Scheme S1). Tetraethylorthosilicate (TEOS, >98%), dimethylformamide (DMF, 99.8%) and hydrochloric acid (37%, analytical grade) were purchased from Sigma-Aldrich, Australia. All chemicals were used without further purification.

Preparation of polymeric soft template

Micelles of PS-P2VP-PEO triblock copolymer were prepared according to the method described earlier.[41] For the typical preparation of micelles, 2 wt.% of the copolymer was dissolved in 5 ml DMF containing 10 wt.% water. The mixture was stirred with a magnetic stirrer until the copolymer was completely dissolved. Subsequent formation of micelles was achieved by eliminating DMF from the solution by dialysis against regularly replaced Milli-Q (MQ) water. Completion of dialysis was confirmed by measuring the surface tension of the MQ water. Finally, the micelles were transferred to a 250 ml standard flask and diluted with MQ water to make the

concentration to 1 g L^{-1}. The micelle structure's formation was confirmed by images obtained using a FEI Quanta 450 FEG field emission scanning electron microscope (FESEM) with an accelerating voltage of 10 kV.

Synthesis of polymer@silica nanocomposite

After preparing the micelles the functional groups were activated by adjusting the pH value of the micelle suspension to 4 with 0.1 M HCl. After adding the desired amount of silica precursor (TEOS) to maintain a molar ratio of TEOS to P2VP around 30:1, the micelle suspension was slowly stirred for 2 days at room temperature. To ensure slow hydrolysis, TEOS was added drop-wise at 0.1 ml min^{-1}. The suspension of the template micelle and the precursor was stored for 4 more days at room temperature without stirring to allow the silica network to be formed by the sol-gel reaction. The resulting polymer@silica (PS-P2VP-PEO/silica) nanocomposite particles were separated from the solvent by centrifugation at 14,000 rpm (19,720x g) and then washed 3 times with MQ water. Finally, the polymer@silica composite was dried at 50 °C for 12 hours.

Formation of porous hollow silica nanospheres

Porous hollow silica nanospheres were obtained by removing the polymeric template from the polymer@silica nanocomposite by calcination in a muffle furnace. The temperature of the furnace was ramped to 550 °C at the rate of 1 °C min^{-1} and retained at 550 °C for 4 h in air. The temperature required for the decomposition of polymer was pre-determined by thermo-gravimetric analysis (TGA). TGA was carried out using a Q600 SDT thermo-gravimetric analyzer (TA Instrument, United States). Approximately 2.5 mg of the polymer@silica nanocomposite sample was heated from 50 to 600 °C in a 40 µl platinum crucible (PN: 960149.901, United States). The heating rate

was 10 °C min^{-1} under an atmosphere of continuous high purity nitrogen gas flowing at 120 ml min^{-1}. The decomposition temperature required for the block copolymer was also ensured by TGA analysis as described above.

Characterization

Micro-morphology analysis. The external surface morphology and elemental composition of synthesized BHSNs and polymer@silica nanocomposite were evaluated using a field emission scanning electron microscope (FESEM, Zeiss Supra 55VP, Carl Zeiss AG) fitted with an energy dispersive X-ray spectroscopy (EDAX) facility. For SEM analysis, all the dried powder samples were placed on a sample holder followed by coating with Au-Pd (8.5 nm) using a Leica EM ACE600 high vacuum coater for high-resolution imaging. The SEM images were generated with an accelerating voltage of 4.5 kV, and multiple image magnifications of various areas of the sample were obtained. The hollow structure of the BHSNs was investigated by using a transmission electron microscope (TEM, Tecnai T20, FEI Tecnai (LaB6)). Before TEM analysis the BHSNs powder sample was dispersed in ethanol followed by drying one drop of BHSNs-containing suspension placed on a copper grid (Ted Pella Inc., CA, USA). The TEM images were carried out at an accelerating voltage of 120 kV. Whereas the high resolution TEM images were taken by using a JEM-2100F (JEOL, USA) transmission electron microscope at an accelerating voltage of 200 kV. The shell thickness and void space of HSNs were evaluated by image analysis using ImageJ software (NIH, free download).

***Fourier transform infrared* spectroscopy.** The functional groups present in the polymer@silica nanocomposite before and after calcination, as well as in the polymeric powder samples, were assessed by attenuated total reflectance Fourier transform infrared (FTIR) spectrometer (ATR-

238 FTIR, IR Afinity-1, Shimadzu, Japan). FTIR analysis was performed in the 4000 to 400 cm^{-1} range
239 with a signal resolution of 4 cm^{-1}. Each sample was scanned 32 times to obtain a good signal to
240 noise ratio.

241 ***X-ray diffraction pattern*** **analysis.** The X-ray diffraction (XRD) pattern of BHSNs was
242 evaluated by a Bruker D8 Discovery X-ray diffractometer equipped with Cu-Kα radiation (λ =
243 0.154 nm) generated at 40 kV and 40 mA. The scanning rate was 1° (2θ) min^{-1} within the scanning
244 range from 1° to 10° and 10° to 80° (2θ) with a step size of 0.04°.

245 ***Hydrodynamic diameter and zeta potential measurement.*** A Zetasizer Nano ZS90 (Malvern
246 Instruments Ltd., UK) operating with a He-Ne laser at a wavelength of 633 nm was used in this
247 study to determine both the zeta potential and hydrodynamic diameter of sample materials. The
248 measurement of zeta potential was achieved by a combination of Laser Doppler Velocimetry and
249 phase analysis light scattering (PALS) with Malvern's patented M3-PALS technique. A blank
250 consisting of ultrapure water (Milli-Q**)**, Millipore, USA) was run systematically before the samples
251 to calibrate the instrument. Zeta potential was measured within the pH range of 4-11. The particles'
252 nanosized diameter was determined by dynamic light scattering (DLS) mode.

253

254 **RESULTS AND DISCUSSION**

255 ***Characterization of polymeric micelle.*** For synthesis of BHSNs, the micelles of PS–P2VP–PEO
256 were prepared initially as described in the experimental section. Figure 1 shows that spherical
257 micelles of PS–P2VP–PEO were successfully formed with a uniform size range. The average
258 diameter of the micelles was 40 ± 3.78 nm (at pH > 5) measured from SEM images using ImageJ
259 software (NIH). In contrast, the average diameter of micelles had a measurement of 64 ± 2.3 nm
260 using the DLS system at low pH (~4), indicating a monodispersed size distribution (Figure 2). The

difference in average diameter was observed in these two methods due to pH responsive behavior of the functional P2VP block. This block mainly consists of aromatic amines such as pyridine. The N atom of pyridine is readily protonated at lower pH (< 5) due to the presence of lone pair electrons (see Supporting Information, Scheme S1). The electrostatic repulsive forces generated among the PVP blocks result in considerable expansion of micelles' diameter.[41] In contrast, the deprotonated P2VP block is reported as being hydrophobic; hence, it collapsed on the PS block at high pH (> 5). In an earlier study, a similar trend was observed as the average diameter of the micelles was found to be 67 nm in the DLS system when produced with a triblock copolymer PS(20.1k)–P2VP(14.2k)–PEO(26.0k), while the average diameter was 42 nm as determined by TEM image analysis.[11] The sizes as well as expanded diameters of micelles also varied depending on the block sizes of the copolymer.[36,42] The effect of pH on micelle size distribution is well described elsewhere.[41]

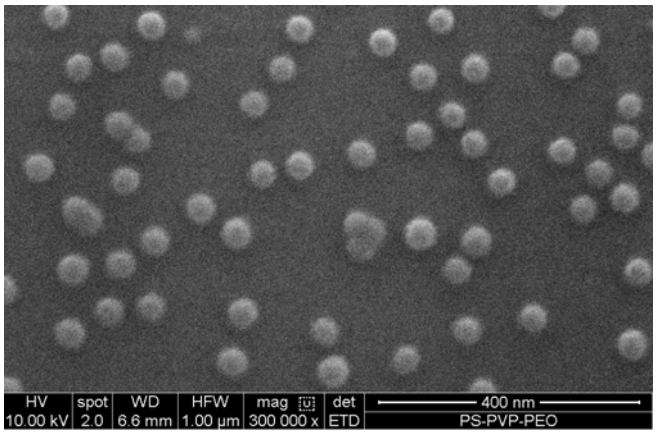

Figure 1. The morphological structure of micelles synthesized using the PS–PVP–PEO block co-polymer as PS(20.0k)–P2VP(15.0k)–PEO(27.0k).

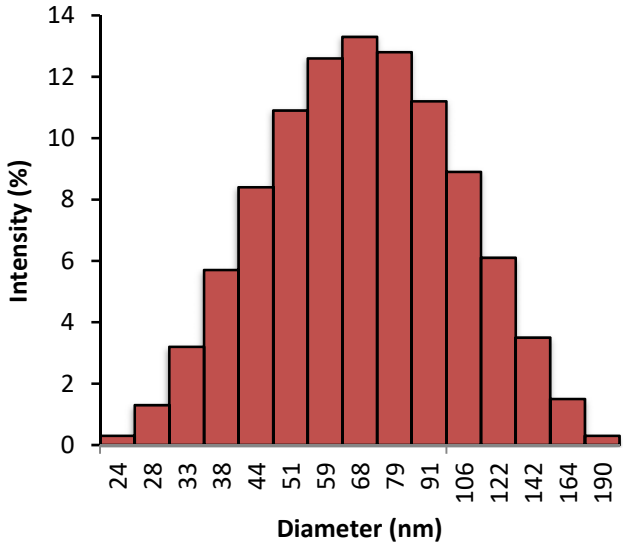

Figure 2. Histogram obtained from the DLS system showing the micelles' diameter and corresponding intensity percentage of the PS–PVP–PEO block co-polymeric micelles at pH 4.

Confirmation of polymer@silica composite structure. To confirm polymer@silica composite structures, and to understand the interactions of silica deposition with the block copolymer, changes in the bonding structures of pristine PS-P2VP-PEO block copolymer as well as polymer@silica composite before and after calcination were evaluated by FTIR analysis (Figure 3). The structure of the block copolymer (PS-P2VP-PEO) is mainly dominated by alkyl and alkoxy groups. For this reason the block copolymer exhibited very strong bands at 2850 cm^{-1} and 1097 cm^{-1} corresponding to C–H stretching vibrations of alkyl (methyl and/or methylene) groups and –C–O–C– stretching vibrations of ethoxy groups of polymer backbone, respectively (Figure 3a).[42-44] The energy bands observed at 1582 cm^{-1} and 1456 cm^{-1} were attributed to >C=C< stretching energies present in the aromatic ring of corresponding phenyl and pyridyl groups that were present in the PS block and P2VP block, respectively, in the polymer backbone.[11,42] The band vibrations corresponding with wavenumbers at 1344 cm^{-1} and 1265 cm^{-1} were due to C–H bending of alkyl

groups of the polymeric chain, whereas band vibrations observed at wavelength number 692 cm^{-1} and 758 cm^{-1} were due to C-H bending of aromatic rings.

The FTIR spectrum of the polymer@silica composite has represented complex band vibrations of block copolymer and silica. (Figure 3b). Significant changes were observed in band vibrations of block copolymer present in polymer@silica composite compared to pristine PS-P2VP-PEO block co-polymer. These changes were caused by deposition of silica over the PS core as well as chemical bonding between silica and the P2PV block. It has previously been shown that polystyrene exhibits characteristic bands around 3001 cm^{-1} for C–H stretching of aromatic rings, 2850 cm^{-1} corresponds to C–H symmetric stretching of alkyl polymeric chains, and band vibration at 1452 cm^{-1} indicates >C=C< stretching of aromatic rings. In addition, the characteristic peaks at 1200-1400 cm^{-1} and 650-780 cm^{-1} were denoted as C-H bending in the aliphatic chain and in the aromatic ring, respectively.[45,46] Conversely, shifting of the characteristic band vibrational peak of >C=C< stretching was related to aromatic phenyl rings of PS to a higher wavenumber (1500-1600 cm^{-1}).[47] This peak shifting was mostly observed when PS was grafted with P2VP to form a block copolymer.

The PS block of the triblock copolymer used in this study is hydrophobic in nature, thus, core of the micelles are formed on dialysis via attractive forces among PS blocks (hydrophobic and π-π interaction) which is required to minimize energetically unfavorable solvophobic interactions.[48] In this condition, band vibrational signal of phenyl group present in PS blocks becomes weak. Whereas polymer@silica composite was formed due to deposition of silica over the core, i.e. PS block, the silica layer may prevent the reception weak band vibrational signal of the PS block. Consequently, all the characteristic peaks of the PS block disappeared in the FTIR spectrum of the polymer@silica composite. Similarly, the band vibrational signal of oleic acid disappeared due to

314 silica deposition forming nanocrystal structure.[49] It is therefore apparent that the band vibration
315 observed at 1525 cm^{-1} is likely to be due to >C=C< stretching of the P2VP block's pyridine rings.
316 The peak appearing at wavenumber 1647 cm^{-1} is representative of the N-H group and indicates the
317 hydrogen bonding interaction between silica and pyridine rings. However, the broad band with
318 peak maxima at 1525 cm^{-1} and 1647 cm^{-1} occurred may due to overlapping of >C=C< stretching
319 of pyridine rings and C–H bending of alkyl groups as well as OH/-NH vibrations[49] respectively
320 (Figure 3b inset). The formation of an N-H bond was also confirmed from the band vibrational
321 peak observed at 2324 cm^{-1} (Figure 3b inset). In their study, Huang et al.[50] observed a similar peak
322 for N-H band vibration of structural amine present in octadecylamine. Furthermore, the symmetric
323 C-H stretching band position at 2850 cm^{-1} shifted to a higher wavenumber (2910 cm^{-1}). The
324 shifting of band position is also indicative of asymmetric stretching of C-H in the polymeric chain
325 of P2VP.
326 Moreover, the shifting of band position provides information on electron transfer to pyridine
327 rings, which ensures their electron resonance when a lone pair electron of N atoms was involved
328 in hydrogen bonding interaction with silanol (Si-OH) or other moieties, such as ethanol
329 (hydrolyzed by-products of TEOS). The newly developed band vibrations at 3832 cm^{-1} and 3740
330 cm^{-1} indicated O-H stretching of Si-OH. However, the band position of the most intensified block
331 copolymeric peak shifted from 1097 cm^{-1} to 1078 cm^{-1} in the FTIR spectrum of the polymer@silica
332 composite. This can be attributed to band vibration for both Si-O-Si and –C–O–C– stretching
333 around this wavenumber, which was confirmed from the FTIR spectrum of the calcined
334 polymer@silica composite sample. In the calcined polymer@silica composite sample, the peak
335 intensity was drastically reduced with further shifting in peak position from 1078 cm^{-1} to 1074 cm^{-1}.
336 This indicated Si-O-Si stretching whereas the reduced peak intensity also highlighted –C–O–C–

337 stretching at 1074 cm^{-1} in the polymer@silica composite. The intensified band vibration at 1074
338 cm^{-1} was attributed to the ethoxy group's strong spectrum signal. It can therefore be assumed that
339 the PEO block was free from silica deposition.

340 Moreover, the FTIR spectrum of the calcined polymer@silica composite sample revealed that
341 along with –C–O–C– stretching band vibration all of the polymeric bands completely disappeared
342 in the calcined polymer@silica composite structure. This left the characteristic vibration bands of
343 pure SiO_2 (Figure 3c), indicating the complete removal of polymer from the polymer@silica
344 composite. In the calcined sample a strong vibration band at 1074 cm^{-1} corresponded to Si–O–Si
345 symmetrical stretching (γ_{sym}) whereas the shoulder growth at 1184 cm^{-1} indicated Si–O–Si
346 asymmetrical stretching (γ_{asym}).[51] Other characteristic band vibrations were observed at 782 cm^{-1}
347 and at 954 cm^{-1} possibly due to symmetric Si-O stretching vibration of Si-O-Si and Si-O stretching
348 vibration bond of Si-OH, respectively.[52] The band vibration at 3832 cm^{-1} and 3740 cm^{-1} of O-H
349 stretching also disappeared in the calcined sample, suggesting that the P2VP block interacted with
350 the Si-OH group of the deposited silica.

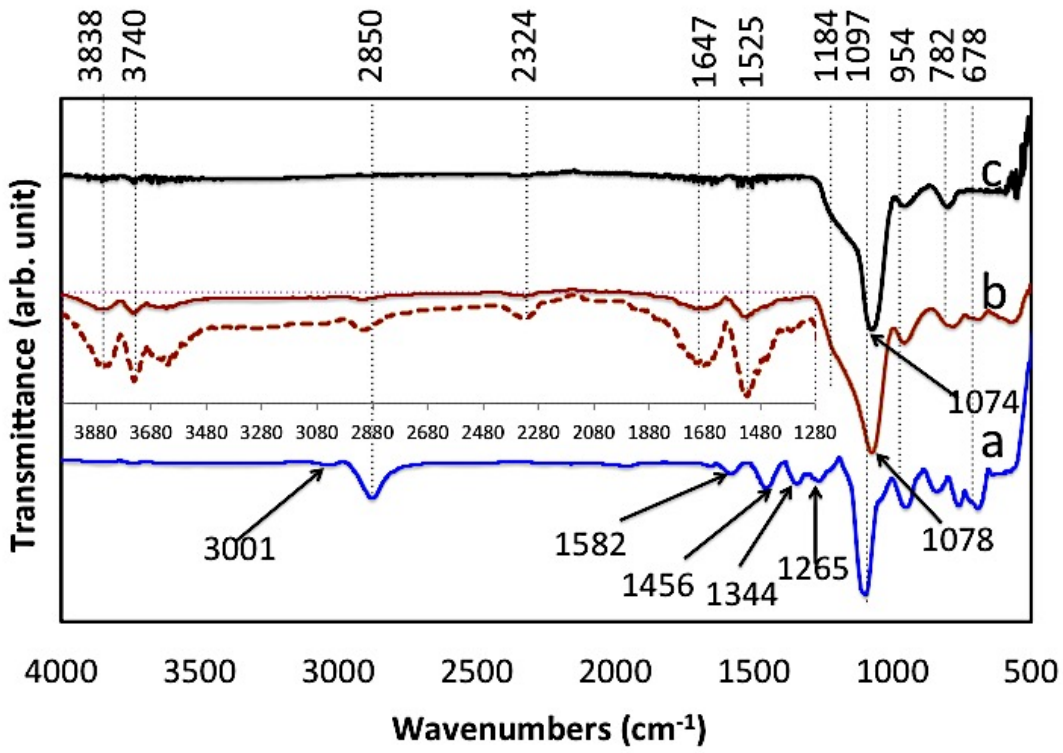

Figure 3. FTIR-ATR spectra of a. PS-PVP-PEO block copolymer, b. Polymer@silica nanocomposite and c. Polymer@silica nanocomposite after calcination.

Thermal analysis. TGA analysis of the triblock copolymer as well as polymer@silica composite before and after calcination was carried out to investigate their thermal behavior and to quantify the amount (wt.%) of block copolymer template present in the composite (Figure 4). Figure 4a illustrates that 100% weight loss was observed for the block copolymeric sample, whereas the corresponding DTG curve demonstrates that the decomposition of the block polymer took place over the temperature range of 300 to 500 °C with the maximum mass loss rate occurring at 408 °C (Figure 4i). In contrast, 43% weight loss was calculated from the TGA curve due to decomposition of the block copolymer for the polymer@silica composite sample (Figure 4b). The DTG curve of the polymer@silica sample indicated the decomposition of polymeric materials from the

363 nanocomposite structure also occurred within the 300-500 °C temperature range. However, the
364 temperature of the maximum mass loss rate shifted to 432 °C (Figure 4ii). In the polymer@silica
365 sample, the peak maximum in the DTG shifted to a higher temperature compared to the polymer,
366 probably due to dehydroxylation through which the P2VP block interacted with silica networks.
367 This outcome also indicated that during core-shell arrangement in polymer@silica composite,
368 silica was deposited on the polymeric core establishing a hydrogen bonding interaction with the
369 P2VP block, which generated structural Si-OH. The FTIR spectrum of the polymer@silica
370 composite also exhibited the specific band vibrations of –OH group (Figure 3b). Conversely, only
371 0.2% weight loss was found for the calcined polymer@silica composite sample and no
372 corresponding specific peak was observed in the corresponding DTG curve (Figure 4iii). From
373 this observation, it is reasonable to assume that total weight loss (around 43%) observed in
374 polymer@silica composite was due to the block copolymer.
375

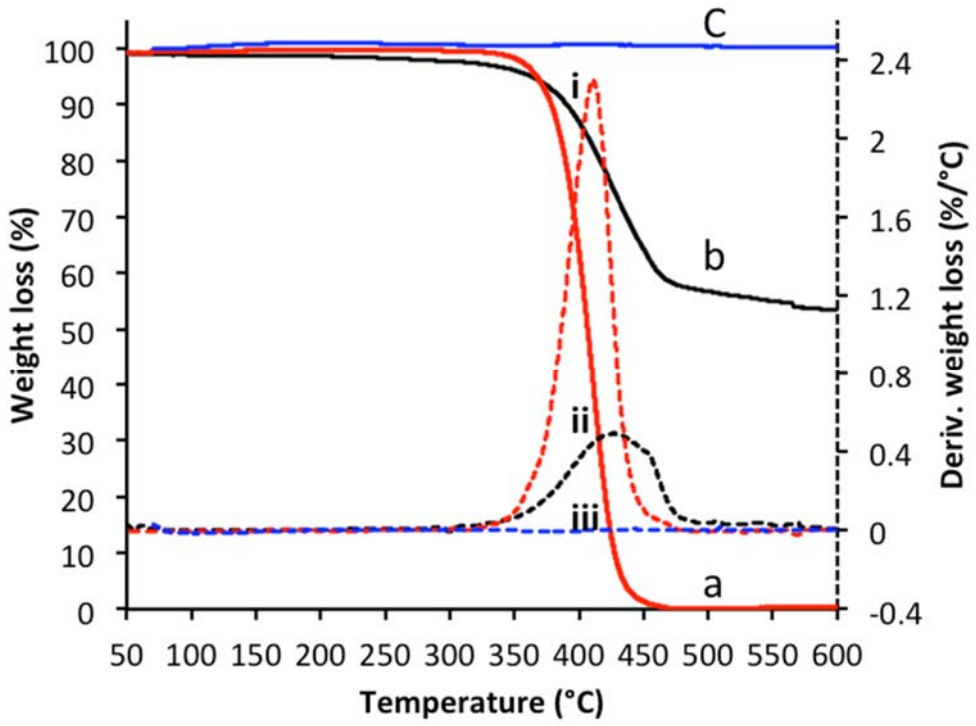

376

377 Figure 4. TGA curves of a. PS-P2VP-PEO block copolymer (red line), b. polymer@silica
378 composite before calcination (black line), c. polymer@silica composite after calcination (blue line)
379 and DTG curves of i. PS-P2VP-PEO block copolymer (dotted red line), ii. polymer@silica
380 composite before calcination (dotted black line), iii. polymer@silica composite after calcination
381 (dotted blue line).

382 ***Elemental analysis.*** The elemental analysis of the polymer@silica composite before and after
383 calcination strongly supports the results obtained by TGA analysis considering the three major
384 elements, i.e. C, O and Si (Figure 5). It was found that the polymer@silica composite contained
385 around 50% C which was drastically reduced to less than 1% by calcination (Table 1). Hence,
386 calcination of the polymeric template completely removed it from the composite structure.
387 Whereas the atomic (%) ratio of O to Si is much greater than 2:1 in the polymer@silica composite,
388 it was almost 2:1 after calcination.

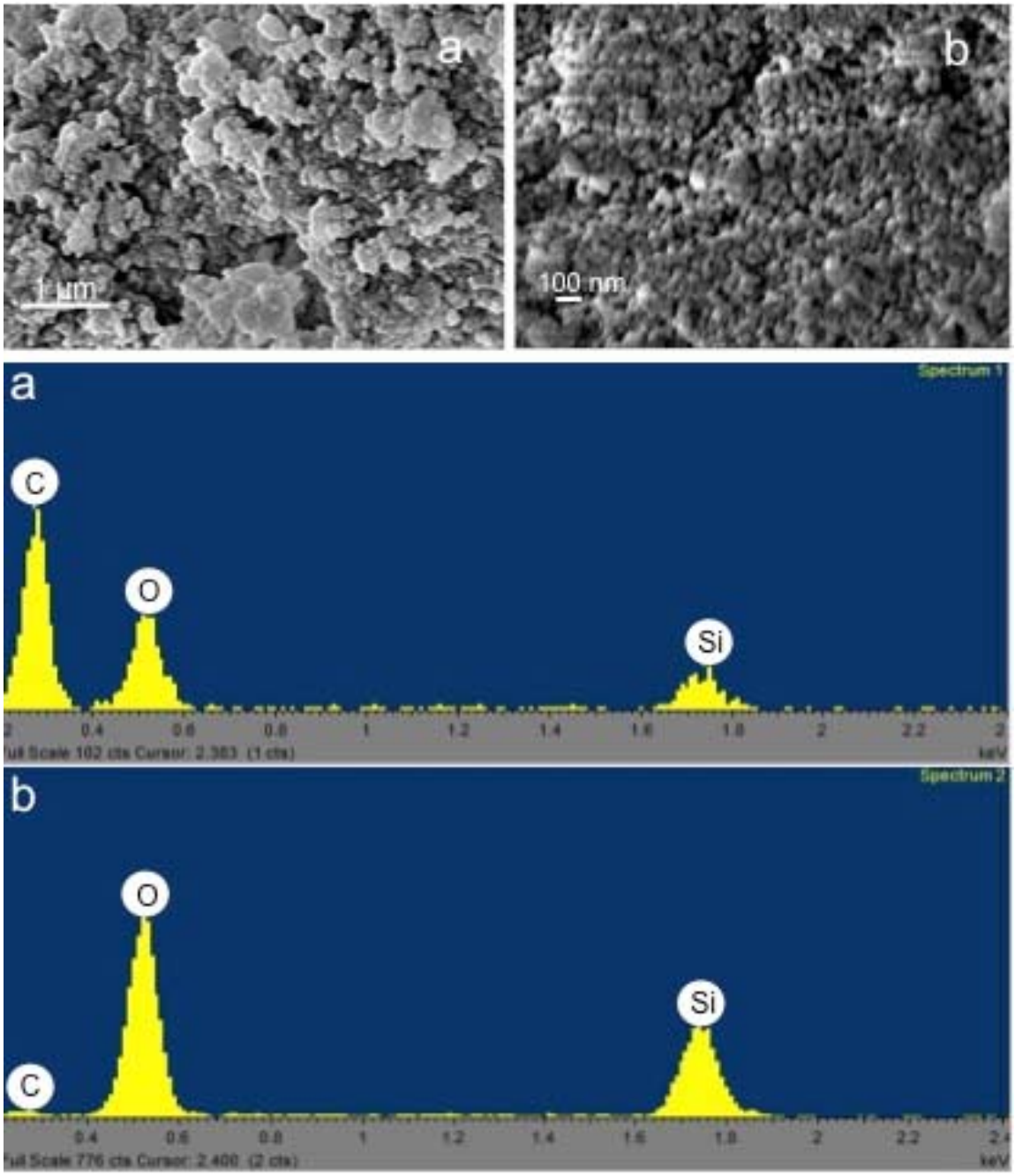

Figure 5. SEM images and EDAX spectrum of polymer@silica composite before calcination (a) and after calcination (b)

Generally, the atomic ratio of O and Si in SiO_2 is 2:1; hence, one can predict from this elemental analysis that due to calcination of the polymer@silica composite the polymeric template was

completely removed it from the composite structure. After calcination SiO_2 is the only material that is present in the composite structure. The ratio of O to Si in the polymer@silica was much greater than 2:1 due to the presence of O containing PEO block in the composite structure. Furthermore, from SEM images, it was observed that before calcination, the polymer@silica composite remained in a highly aggregated state that changed to a dispersed or loosely aggregated following calcination of the composite (Figure 5). This phenomenon supports the assumption of FTIR analysis that during polymer@silica formation the PEO block was free from silica deposition and mainly acted as a barrier between the silica nanospheres. Therefore, homogeneously distributed and uniform silica nanospheres were formed. The uniform size-distribution of silica nanospheres was further confirmed by TEM analysis as well as an assessment of particle size distribution of synthesized silica nanospheres using the DLS system.

Table 1: Elemental composition of polymer@silica nanocomposite before and after calcination determined by EDAX analysis

Material status	C		O		Si	
	Weight %	Atomic %	Weight %	Atomic %	Weight %	Atomic %
Polymer@silica (Before calcination)	51	62	32	29	17	9
Polymer@silica (After calcination)	1	1	55	68	44	31

Micro-morphology of synthesized silica nanospheres. Complete decomposition of the polymeric template by calcination was further confirmed by TEM (Figure 6a). Figure 6a shows that all the hollow-structured silica nanospheres were spherical with a uniform size, contained

large void spaces and had homogeneous size distribution. Based on the image analysis the average particle size was estimated as 41.87 ± 3.28 nm, the average void space was 21.71 ± 1.22 nm, and the average shell thickness was 10.17 ± 1.68 nm. Earlier studies indicated that the size of the void spaces was correlated with the chain length of the PS block, while an increasing trend in size of void spaces was observed with increasing molecular weight of the PS block.[36,44] Gohy et al.[41] measured the size of the PS core of the PS(20.1k)–P2VP(14.2k)–PEO(26k) micelle as 20 nm. We also observed the micelles' diameter as 20 nm (83.6%) when the image was analyzed using FESEM (see Supporting Information, Figure S1). Therefore it is reasonable to conclude that the void space of the synthesized HSNs is mainly structured with the PS block. In addition, shrinkage of the core also occurred during silica condensation, and consequently an expanded core diameter may be often observed by micro-morphology and DLS analysis. Shrinkage of hollow silica particles during calcination is also a common phenomenon while they are synthesized using a polymeric soft template. Rough outer surfaces were also observed indicating the presence of mesopores in the shell wall. Along with mesopores, the presence of large single pore on shell was confirmed from Figure 6b. Furthermore, TEM image analysis indicated the average diameter of the large pore on shell as 15.95 nm (see Supporting Information Figure S2). The SEM image of BHSNs also confirmed that the synthesized silica nanospheres were spherical in shape and homogeneously distributed (Figure ~~6b~~6c). Furthermore, the SEM images also depicted single large pore openings in the silica nanospheres, indicating the successful synthesis of bowl-structured hollow silica nanospheres (BHSNs) (Figure ~~6b~~6c). However, only a small fraction of the BHSNs possess such characteristic under electron microscopy due to morphological orientation of the particles.[53] The single large opening or hole was observed only in SEM image when the nanospheres deposited with keeping the large single pore or hole towards electron beam. In other

positions, it was not possible to detect via SEM. Similar limitation was also observed for TEM analysis and only the pore openings could be observed when the pore openings are faced horizontally. From the available literature, similar phenomenon was observed for different nanoparticles containing large through holes on shell.[54-56] The mesoporous shell can also be proved by the nitrogen adsorption-desorption isotherm (see Supporting Information Figure S3a), which exhibits typical type-IV hysteresis loop. Additionally, the Barrett–Joyner–Halenda (BJH) pore size distribution plot (see Supporting Information Figure S3b) indicates the presence of various size mesopores.

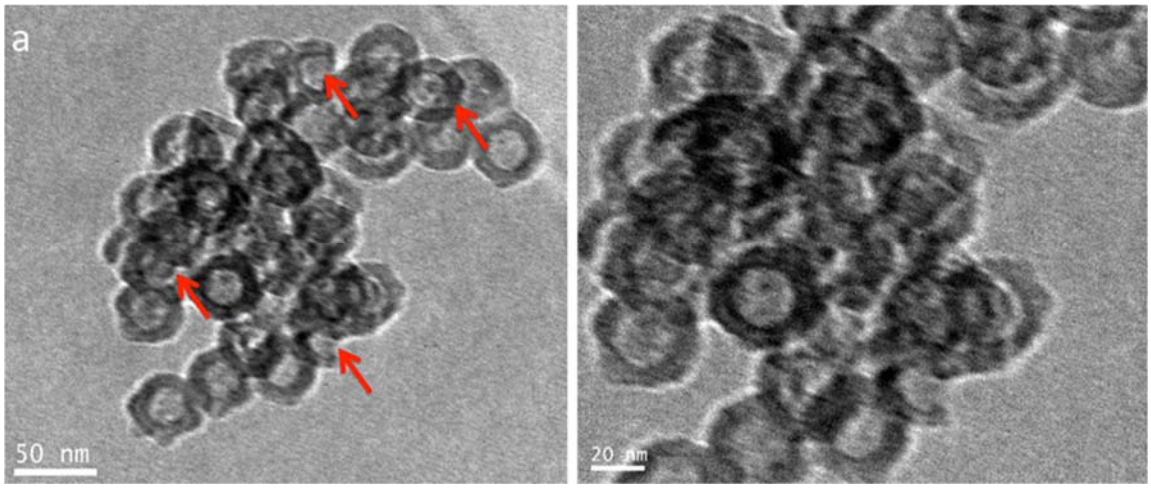

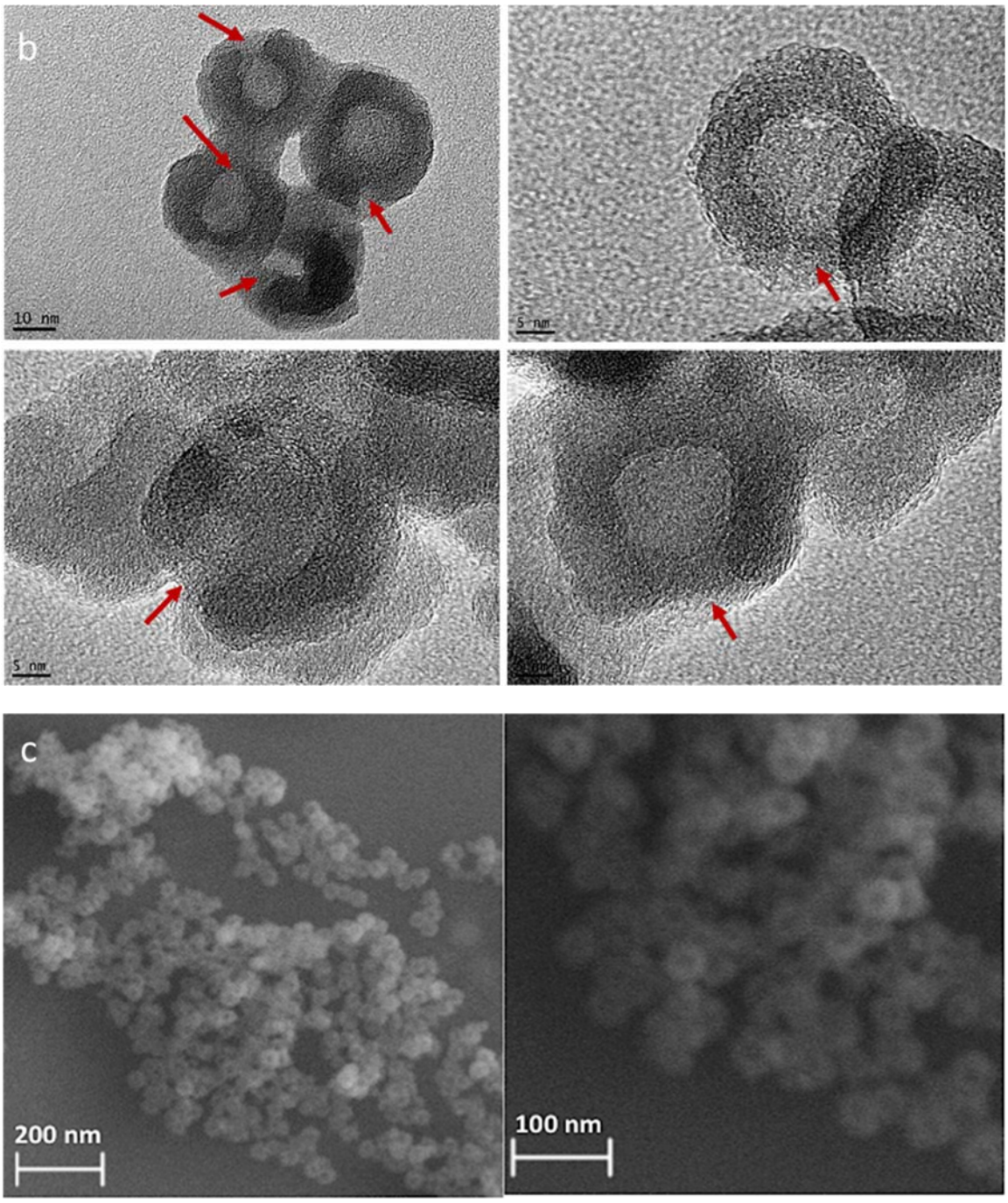

Figure 6. TEM images showing uniform size distribution of silica nanospheres with large void spaces (a), HRTEM images showing large single pore on shell (b) and SEM images showing large pore openings (c). Red arrows indicate pore openings in the shell.

X-ray diffraction pattern of BHSNs. The powder XRD patterns of the synthesized BHSNs are presented in Figure 6. The appearance of diffraction peaks 2θ between 1 to 2 degrees indicates the presence of mesopores on the surface (Figure 7a). A broad diffraction peak at 2θ angle between 2 to 3.2, conversely, suggests the possibility of a large porous structure consisting of hollow spherical particles, further confirming SEM observations of large pore openings in the shell. The d-spacing value indicated the average pore size was around 9 nm. However, the XRD pattern at higher 2θ angle highlighted a single broad peak centered at approximately 23°, which is characteristic of the diffraction of amorphous silica (Figure 7b). This peak is possibly indicative of a mesostructure of synthesized silica.[51] No other peak was observed throughout the 2θ angle (from 1 to 80 degrees) indicating that the synthesized material is pure silica free from impurities.

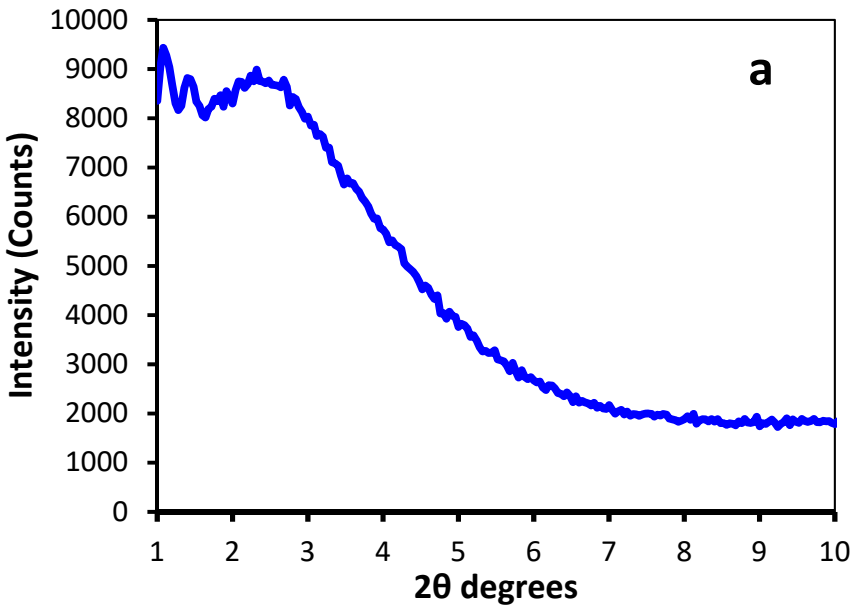

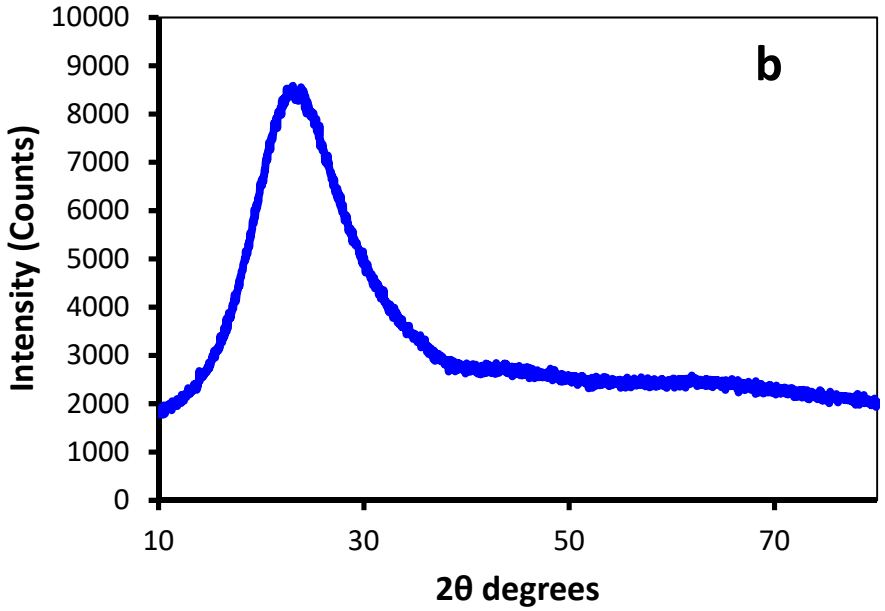

Figure 7. XRD patterns of synthesized BHSNs obtained by using the PS-P2VP-PEO block copolymer a. lower angle and b. at higher angle

Zeta potential and surface chemistry. To investigate the surface chemistry of BHSNs, zeta potential values were measured over a wide range of pH (4-11). During this process, the initially suspended pH of BHSNs was adjusted at different pH levels followed by equilibration at room temperature for 12 h. After equilibration the final pH was measured and the corresponding zeta values were determined. The zeta values and the final pH are presented in Figure 8a. From Figure 8a, it is apparent that the negative zeta value of BHSNs increased when the pH of the aqueous suspension increased. From XRD analysis it is clear that the structures of the synthesized BHSNs are predominantly amorphous and apparently similar to pure silica. Silica is inherently an acidic oxide; the pH of an aqueous suspension of silica is slightly acidic. When exposed to water, partial or total particle surface hydroxylation can cause the formation of silanol groups such as Si(OH)n. Such silanol groups may dissociate in pure water through the following reactions:

$$\equiv Si\text{-}OH + OH^- \rightarrow Si\text{-}O^- + H_2O \ (pH > 9.0) \qquad \text{(eq. 1)}$$

$\equiv Si\text{-}OH + H^+ \rightarrow Si\text{-}OH_2^+ (pH<2.0)$ (eq. 2)

Following eq. 1, the Si-OH normally tends to act as a proton donor in aqueous solution and becomes negatively charged. With increasing pH the silica surfaces become more negatively charged. Under low pH conditions Si-OH tends to become protonated and the degree of protonation increases with decreasing pH of the aqueous suspension (eq. 2). Si-OH only remains in a fully protonated state at an extremely low pH value (< 2). Therefore, over a wide range of pH, SiO_2 exhibits a negative surface charge in aqueous medium. Changes in initial pH of BHSNs after 12 h also indicated their similar surface properties. The differences between initial and final pH are presented in Figure 8b. It was observed that the final pH values increased when the initial system pH was below pH ~4.5. However, the opposite results were observed in suspensions with an initial pH above 4.5. Therefore, it can be assumed that the synthesized BHSNs acted as a proton acceptor at lower pH whereas they were deprotonated at higher pH. According to Figure 8b, it can also be concluded that the degree of deprotonation of BHSNs is much larger than protonation. Deprotonation of Si-OH groups at water-silica interfaces is important for binding ions and molecules to their surfaces.[57] The surface charge behavior of BHSNs demonstrates their ability to establish significant columbic or electrostatic interactions with positively charged molecules at higher pH.

494

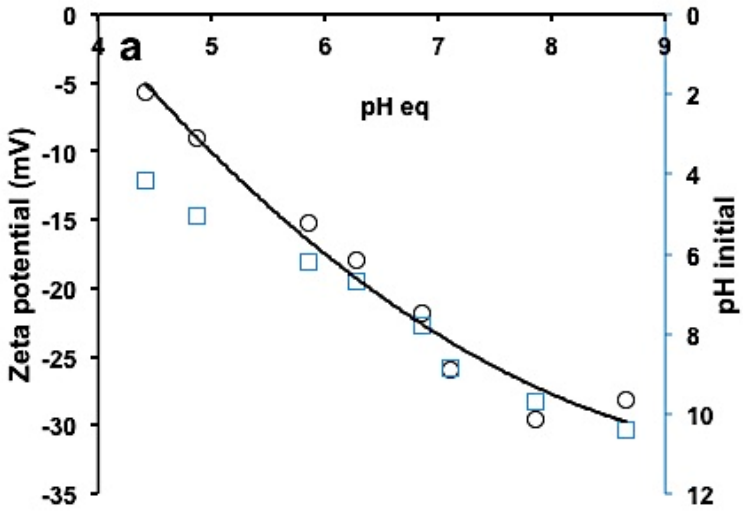

495

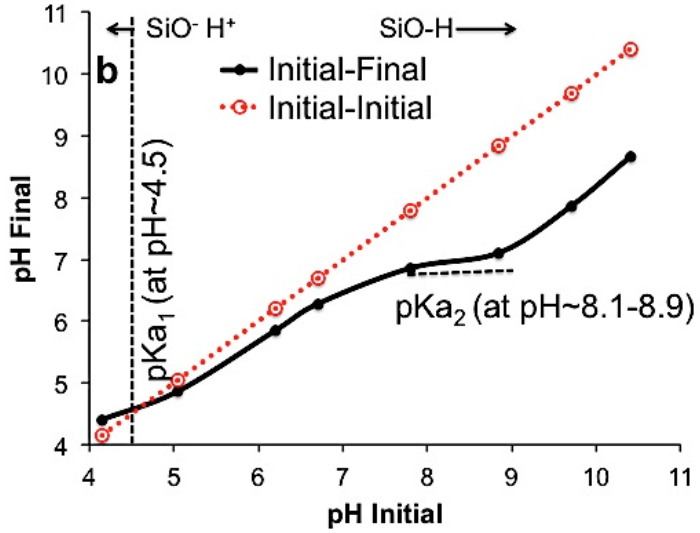

496 Figure 8. Showing (a) zeta potential and (b) protonated-deprotonated behavior of BHSNs in
497 aqueous media at different pH conditions.

498 ***Particle size of BHSNs.*** In addition to surface properties, the ability of nanomaterials to disperse
499 is also important to achieve the desired performance. Hence, the diameter of BHSNs was further
500 investigated using the DLS system. Considering the higher zeta values of BHSNs at higher pH,
501 the suspension pH was adjusted to 11.2. In the DLS system monodispersed particle size

distribution was observed where the z-average particle size was 44.61 nm (Figure 9). This average particle size proved to be similar to the average particle size observed through TEM image analysis (Figure 6a). This finding indicates that the synthesized BHSNs are able to completely disperse in aqueous solutions at higher pH because of their high negative surface charge where the electrostatic repulsion force is more prominent among the nanospheres.

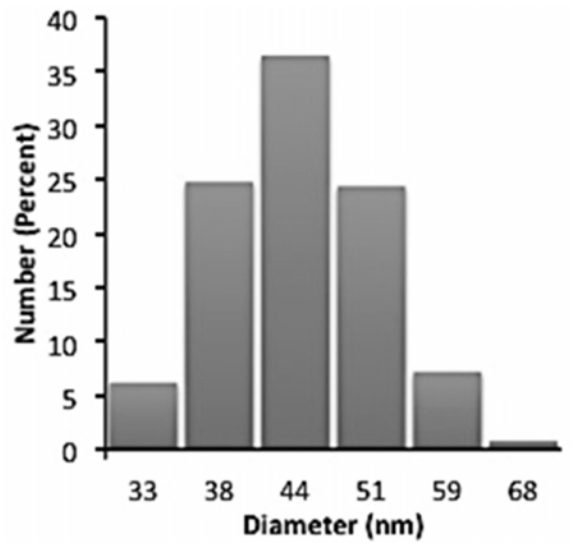

Figure 9. Histogram obtained from the DLS system showing the particle size distribution of BHSNs and corresponding number percentage.

Mechanism of synthesis

Under acidic (pH <5) or basic (pH>8) conditions the synthesis of silica by the sol-gel process from organo-silicates such as TEOS proceeds through hydrolysis and condensation steps. These can be described by equations 3 and 4.[58,59]

Hydrolysis of TEOS:

$$Si(OC_2H_5)_4 + 4H_2O \rightarrow Si(OH)_4 + 4C_2H_5OH \quad \text{(eq. 3)}$$

Condensation step:

$$Si(OH)_4 \rightarrow SiO_2 + 2H_2O \quad \text{(eq. 4)}$$

However, the processes are deemed to occur through several steps on a suitable template such as: (1) fast hydrolysis catalyzed by highly acidic (e.g., in the presence of HCl) or basic (e.g., in the presence of NH_3) aqueous solution; (2) condensation of $Si(OH)_4$ to form silica-coated template spheres; (3) condensation of $Si(OH)_4$ to form free silica nanoclusters; (4) capture of free silica nanoclusters onto the template; and (5) aggregation of free silica nanoclusters into unwanted and irregular aggregates of silica.[60] It is essential to prevent the irregular aggregation that is driven by fast hydrolysis of TEOS in the presence of diluted HCl in aqueous solution.[60] It is expected that slow hydrolysis along with condensation of silica over a template could avoid such aggregation, while ensuring the absence of a free catalyst in the solution.[61]

So far, core-shell-corona structured micelles of ABC triblock co-polymer (PS-P2VP-PEO) have demonstrated their potential as a template for synthesis of HSNs where core-shell interfaces of the micelles played the vital role in silica growth and deposition over micelles' core. Thus, the void spaces of synthesized BHSNs were primarily depended on the core size of the micelles. Due to the hydrophobic nature of the PS block the rigid core structure of the micelles was formed during the dialysis process; it remained unchanged throughout the sol-gel reactions required for core-shell arrangement as polymer@silica composite formation. Therefore the PS blocks were employed to construct hollow interiors of BHSNs. Earlier studies showed that the size of the void spaces was correlated with the chain length of the PS block, while an increase in the size of void spaces was observed with increasing molecular weight of the PS block, i.e. chain length of the block.[36,44] In addition, shrinkage of the core occurred during condensation process. Shrinkage of hollow silica particles during calcination is also a common phenomenon while they are being synthesized using a polymeric soft template.

The pH responsive functional P2VP block of the copolymer played a significant role in the hydrolysis and condensation of TEOS in the sol-gel process. The P2VP block was ionized at low pH (< 5) and not only captured free silica nanoclusters onto the template but also acted as an acid catalyst during hydrolysis of TEOS. This was followed by controlled condensation of $Si(OH)_4$ to form silica-coated template spheres. The role of the P2VP block in hydrolysis and polycondensation of TEOS is described in Supporting Information (Schemes S2 and S3). Inner smooth surface and rough outer surfaces of BHSNs (Figure 1a, Supporting Information Figure ~~S5~~S6) indicated the condensation of $Si(OH)_4$ on the PS block, condensation of $Si(OH)_4$ to form template-free nanoclusters as well as the capture of free silica nanoclusters onto the template. Herein, no other catalyst was required which ensured that no free catalyst was present in the synthesis media. Subsequently it prevented the irregular aggregation of silica in the solution. Therefore the core-shell arrangement of polymer@silica was successfully formed. This result was also supported by the TEM images of BHSNs since no rigid-structured silica nanoparticles were observed (Figure 6a, 6b). As the growth and deposition of silica on the template was facilitated by the P2VP block, subsequently the TEOS: P2VP molar ratio proved critical in controlling the shell thickness of silica nanospheres. PEO is also able to interact with silanol groups (Si– OH) of silica prominently through hydrogen bonding but only in extremely acidic conditions (pH 1).[62] Hence, we believe that the PEO block was free from silica deposition and growth of silica networks was exclusively formed interacting with P2VP block of the micelles.

In this study, along with hollow spherical nanostructured silica spheres, a single large opening or hole was observed in the shells (Figure ~~6b~~6c). The silica nanospheres have been designated bowl-structured hollow silica nanospheres (BHSNs) due to their large openings (~15 nm) in relation to their small particle size (~45 nm). Synthesis of BHSNs using ABC tri-block

564 copolymeric micelles as a soft template has not yet been reported but hollow-structured
565 mesoporous silica nanospheres have already been successfully synthesized.[11,35,37,42] So far,
566 depending on large pore openings in the shells, silica nanospheres synthesized in earlier studies
567 had different structure. For example, in earlier studies, such material was denoted as 'silica
568 nanobottle' and this may be due to the relatively large particle size compared to the pore
569 openings.[63,64] However, what caused the formation of single large pores on the shells is still
570 unclear. In an earlier study, Zhang et al.[63] assumed that the hole or large pore in the spheres was
571 formed during calcination. This was attributed to the high pressure resulting from polymeric
572 decomposition with this playing an active role in the formation of such pore structures in silica
573 nanospheres.[63]

574 It is important to note that the decomposition of the polymeric template could play a key role
575 when the shell is solid and unable to form mesopores; in most cases, the shells are broken down.[4]
576 It is also reasonable to conclude that if high pressure plays a key role in large pore formation then
577 such a structure would be developed in each case while a hollow structure is obtained from the
578 sacrificial polymeric templating approach through calcination. However, this has not been
579 commonly observed.[51,65] It is therefore possible that not only high-pressure generation during
580 calcination but also other mechanisms are involved in single large pore formation. The main
581 difference between this study and those reported in the literature for synthesizing HSNs is the use
582 of an organosilicate precursor, i.e. TEOS instead of TMOS where similar types of ABC triblock
583 copolymer were used. From morphological differences between synthesized HSNs using these
584 precursors (see Supporting Information Figure S43-S65), it can be assumed that the chemical
585 behavior of the precursor or their by-product played a significant role in the formation of large
586 pore openings, which is consistent with the recent investigations conducted by Yi et al.[64] In their

study, a silica nanobottle with an extended neck and having a 'flask bottle' shape was synthesized.[64] Interestingly, the particle shape and size completely being changed with the replacement of precursor materials has been reported elsewhere.[64]

Considering the observations of Yi et al.[64], we therefore postulate that a by-product of TEOS hydrolysis, such as ethanol, played a pivotal role in the formation of bowl-structured hollow silica nanospheres. The chemical structure of ethanol includes both hydrophilic (-OH group) and hydrophobic (hydrocarbon chain) moieties. In this study, ethanol generated from hydrolysis of TEOS possesses a high affinity for the hydrophobic surface of the micelles' PS core better than water, yet ethanol is more hydrophobic than the PEO block, i.e. corona of the micelles.[66] Therefore, once ethanol is produced as a hydrolyzed by-product of TEOS, it remains at the PS-water interfaces of micelles in an aqueous suspension. Further deposition of silica over the PS block enhanced shell growth and ethanol tended to exude from PS surfaces, but aggregated together on micelles' core due to hydrogen bonding affinity of ethanol to ethanol. During the final stage of shell formation the accumulated ethanol extended throughout the P2VP block to form droplets. The highly accumulated ethanol may also interact with P2VP by hydrogen-bonding and the accumulated ethanol droplets also facilitate gel formation of the PEO block of the micelles[67] which may be responsible for particles' aggregation, as observed in Figure 5a.

In the FTIR spectrum, an intensified peak growth was observed in the polymer@silica nanocomposite compared to the block copolymer at 1078 cm^{-1},[68] whereas the presence of -OH band vibrations indicated the possible existence of ethanol (Figure 2a). Consequently, accumulated ethanol molecules prevented the deposition of silica over the PS block and bowl-structured hollow porous silica nanospheres were observed after calcination of the polymer@silica composite. For

this reason the ethanol/water ratio is an important factor for the deposition of silica over PS.[69] The postulated mechanisms for the synthesis of such a structure are illustrated in Scheme 1.

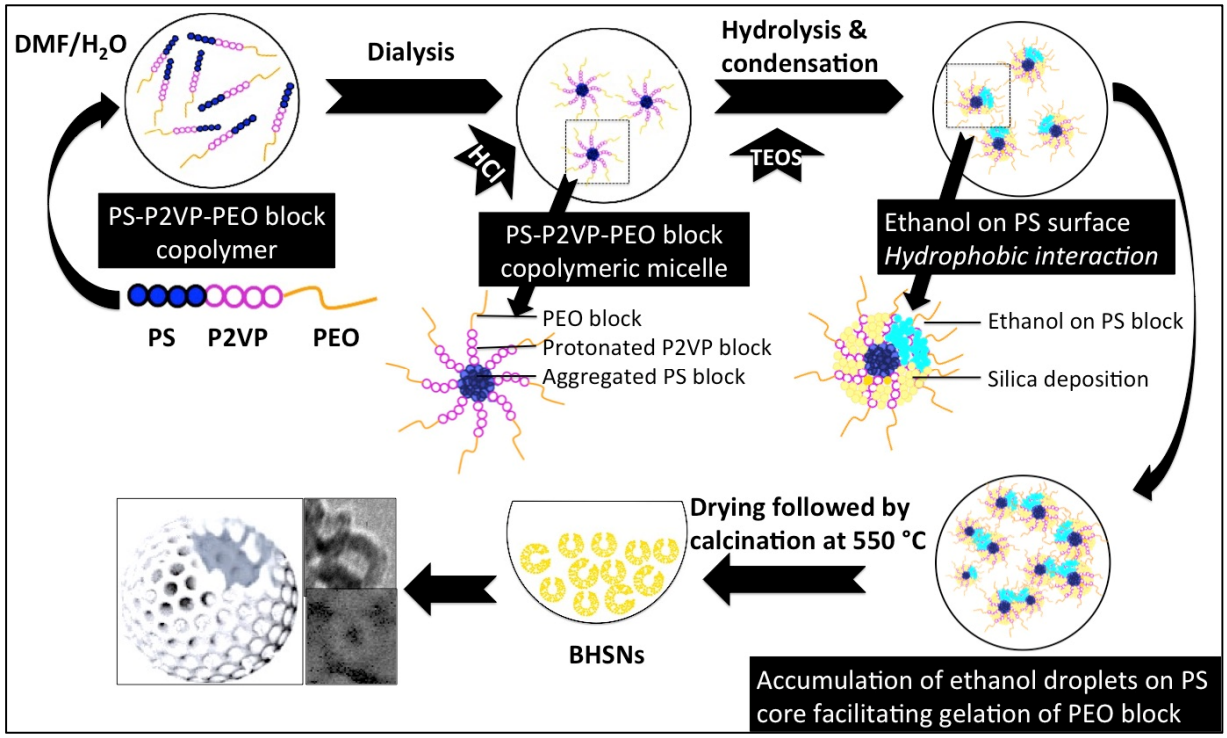

Scheme 1: Postulated mechanisms of bowl-structured hollow silica nanosphere synthesis

CONCLUSIONS

In this study, HSNs with large through-hole or pore openings in the shell were successfully synthesized using core-shell-corona structured micelles of a self-assembled ABC tri-block copolymer (PS-P2VP-PEO) as a soft template. Due to the large pore openings in the shells, the synthesized HSNs were termed as bowl-structured hollow porous silica nanospheres (BHSNs). In this process, core-shell interfaces of the micelles played the key role in deposition and growth of silica (SiO_2) shells on to micelles' core. Herein, protonated the P2VP block not only acted as an acid catalyst during hydrolysis of the precursor, namely, TEOS but also initiated the condensation

622 of a hydrolyzed precursor by acting as a proton-transferring agent. P2VP also played a vital role
623 via binding or capturing the silica nanoclusters onto the PS block and preventing their unwanted
624 growth in the solution. The presence of catalytic moieties on the template's surface led to the
625 formation of silica shell growth on the micelles' core surface. As a result, core-shell
626 nanocomposites structure of polymer@SiO_2 was formed via a simple sol-gel method where the PS
627 block of the triblock copolymer acted as the core. Consequently, a hollow structure was obtained
628 by selective removal of the polymeric cores through the calcination process.
629 The morphology, structure, and composition of the BHSNs produced were determined and
630 characterized by TEM, SEM, FTIR spectroscopy, TGA, XRD, zeta potential analyzer and by a
631 DLS system. TEM images revealed a spherical hollow structure with an average particle size of
632 41.87 ± 3.28 nm, similar to average particle sizes observed in DLS analysis (44.61 nm). The
633 average diameter of void spaces was 21.71 ± 1.22 nm and the shell thickness was 10.17 ± 1.68
634 nm. The average pore size was determined as 15.95 nm. SEM images further confirmed their bowl-
635 structure with a large single pore, or opening, in shells. The large pores in shells were formed due
636 to the prevention of silica growth on the core by the action of accumulated hydrolyzed by-products
637 of TEOS, i.e. ethanol on PS core and slow hydrolysis process. In this case, accumulation of ethanol
638 on micelles core was initiated via hydrophobic interaction caused by the hydrophobic nature of PS
639 and interaction among the ethanol molecules. This established the hydrogen-bonding interaction
640 among them as well as with the P2VP block that may have created gelation of PEO**.** XRD analysis
641 also indicated a disordered mesoporous structure, i.e. the synthesized BHSNs were amorphous.
642 The zeta values indicated that the synthesized BHSNs possess similar surface properties to
643 amorphous silica and a highly negative charge at higher pH. It is expected that the BHSNs

produced may have advantages over HSNs for applications as a carrier for active molecules during loading via the simple immersion method due to their large pore openings.

ASSOCIATED CONTENT

Supporting Information. The following file is available free of charge. It contains further details of chemical structure of the PS-P2VP-PEO block copolymer, micelles core size measurement procedure, the catalytic effect of P2VP block during hydrolysis and condensation of TEOS, pore size measurement of synthesized BHSNs, surface area and surface pore size analysis and morphological differences of HSNs synthesized using TMOS and TEOS (PDF)

AUTHOR INFORMATION

Corresponding Author

*Ravi Naidu

E-mail: Ravi.Naidu@newcastle.edu.au; Ravi.Naidu@crccare.com; **Tel: +61-02-4913 8705**

Notes

The authors declare no competing financial interest.

ACKNOWLEDGMENT

The first author is grateful, firstly, to the University of Newcastle for the University of Newcastle Postgraduate Research Scholarship (UNIPRS), and to the Cooperative Research Centre for Contamination Assessment and Remediation of the Environment (CRC CARE) for scholarship funding. The first author is also grateful to University of Technology Sydney (UTS) for providing support during characterization of the samples.

ABBREVIATIONS

BHSNs, bowl-structured hollow porous silica nanospheres; CRFs, Controlled-release formulations; DLS, Dynamic light scattering; EDAX, Energy dispersive X-ray spectroscopy; FESEM, Field emission scanning electron microscopy; FTIR, Fourier transform infrared; HSNs, hollow porous silica nanospheres; MQ, Milli-Q; PEO, Polyethylene oxide; PS, Polystyrene; P2VP, Poly-2-vinyl pyridine; SCF, Supercritical Fluid; SEM, Scanning electron microscopy; TEM, Transmission electron microscopy; TEOS, Tetraethylorthosilicate; TGA, Thermo-gravimetric analysis; TMOS, Tetramethylorthosilicate; XRD, X-ray diffraction.

REFERENCES

(1) Caruso, F. Nanoengineering of Particle Surfaces. *Advanced Materials* **2001,** *13* (1), 11.

(2) Vafayi, L.; Gharibe, S. Investigation of In Vitro Drug Release from Porous Hollow Silica Nanospheres Prepared of ZnS@SiO2 Core-Shell. *Bioinorganic Chemistry and Applications* **2013,** *2013*, 541030 (6 pages).

(3) Sasidharan, M.; Nakashima, K. Core–Shell–Corona Polymeric Micelles as a Versatile Template for Synthesis of Inorganic Hollow Nanospheres. *Accounts of Chemical Research* **2014,** *47* (1), 157.

(4) Zhang, L.; D'Acunzi, M.; Kappl, M.; Auernhammer, G. K.; Vollmer, D.; van Kats, C. M.; van Blaaderen, A. Hollow Silica Spheres: Synthesis and Mechanical Properties. *Langmuir* **2009,** *25* (5), 2711.

(5) Tang, F.; Li, L.; Chen, D. Mesoporous Silica Nanoparticles: Synthesis, Biocompatibility and Drug Delivery. *Advanced Materials* **2012,** *24* (12), 1504.

(6) Wibowo, D.; Zhao, C.-X.; Peters, B. C.; Middelberg, A. P. J. Sustained Release of Fipronil Insecticide in Vitro and in Vivo from Biocompatible Silica Nanocapsules. *Journal of Agricultural and Food Chemistry* **2014,** *62* (52), 12504.

(7) Wen, L.-X.; Li, Z.-Z.; Zou, H.-K.; Liu, A.-Q.; Chen, J.-F. Controlled release of avermectin from porous hollow silica nanoparticles. *Pest Management Science* **2005,** *61* (6), 583.

(8) Liu, F.; Wen, L.-X.; Li, Z.-Z.; Yu, W.; Sun, H.-Y.; Chen, J.-F. Porous hollow silica nanoparticles as controlled delivery system for water-soluble pesticide. *Materials Research Bulletin* **2006,** *41* (12), 2268.

(9) Li, Z.-Z.; Xu, S.-A.; Wen, L.-X.; Liu, F.; Liu, A.-Q.; Wang, Q.; Sun, H.-Y.; Yu, W.; Chen, J.-F. Controlled release of avermectin from porous hollow silica nanoparticles: Influence of shell thickness on loading efficiency, UV-shielding property and release. *Journal of Controlled Release* **2006,** *111* (1–2), 81.

(10) Nomura, T.; Morimoto, Y.; Tokumoto, H.; Konishi, Y. Fabrication of silica hollow particles using Escherichia coli as a template. *Materials Letters* **2008,** *62* (21–22), 3727.

(11) Sasidharan, M.; Zenibana, H.; Nandi, M.; Bhaumik, A.; Nakashima, K. Synthesis of mesoporous hollow silica nanospheres using polymeric micelles as template and their application as a drug-delivery carrier. *Dalton Transactions* **2013,** *42* (37), 13381.

(12) Dezhi, N.; Lei, W.; Yunhui, S.; Zhengrong, G.; Sen, Y.; Kebin, Z. Amphiphilic Hollow Carbonaceous Microspheres with Permeable Shells. *Angewandte Chemie International Edition* **2010,** *49* (25), 4223.

(13) Shi, Z.-G.; Guo, Q.-Z.; Liu, Y.-T.; Xiao, Y.-X.; Xu, L. Drug delivery devices based on macroporous silica spheres. *Materials Chemistry and Physics* **2011,** *126* (3), 826.

(14) Bao, Y.; Shi, C.; Wang, T.; Li, X.; Ma, J. Recent progress in hollow silica: Template synthesis, morphologies and applications. *Microporous and Mesoporous Materials* **2016,** *227*, 121.

(15) Wei, J.; Sun, Z.; Luo, W.; Li, Y.; Elzatahry, A. A.; Al-Enizi, A. M.; Deng, Y.; Zhao, D. New Insight into the Synthesis of Large-Pore Ordered Mesoporous Materials. *Journal of the American Chemical Society* **2017,** *139* (5), 1706.

(16) Si, Y.; Chen, M.; Wu, L. Syntheses and biomedical applications of hollow micro-/nano-spheres with large-through-holes. *Chemical Society Reviews* **2016,** *45* (3), 690.

(17) Solberg, S. M.; Landry, C. C. Adsorption of DNA into Mesoporous Silica. *The Journal of Physical Chemistry B* **2006,** *110* (31), 15261.

(18) Yufang, Z.; Jianlin, S.; Weihua, S.; Xiaoping, D.; Jingwei, F.; Meilin, R.; Yongsheng, L. Stimuli-Responsive Controlled Drug Release from a Hollow Mesoporous Silica Sphere/Polyelectrolyte Multilayer Core–Shell Structure. *Angewandte Chemie* **2005,** *117* (32), 5213.

(19) Mei, X.; Chen, D.; Li, N.; Xu, Q.; Ge, J.; Li, H.; Lu, J. Hollow mesoporous silica nanoparticles conjugated with pH-sensitive amphiphilic diblock polymer for controlled drug release. *Microporous and Mesoporous Materials* **2012,** *152*, 16.

(20) Argyo, C.; Weiss, V.; Bräuchle, C.; Bein, T. Multifunctional Mesoporous Silica Nanoparticles as a Universal Platform for Drug Delivery. *Chemistry of Materials* **2014,** *26* (1), 435.

(21) Ge, X.; Ge, X.; Wang, M.; Liu, H.; Fang, B.; Li, Z.; Shi, X.; Yang, C.; Li, G. One-Pot Synthesis of Colloidal Nanobowls and Hybrid Multipod-like Nanoparticles by Radiation

Miniemulsion Polymerization. *Macromolecular Rapid Communications* **2011,** *32* (20), 1615.

(22) Mo, A. H.; Landon, P. B.; Emerson, C. D.; Zhang, C.; Anzenberg, P.; Akkiraju, S.; Lal, R. Synthesis of nano-bowls with a Janus template. *Nanoscale* **2015,** *7* (2), 771.

(23) Mandal, S.; Sathish, M.; Saravanan, G.; Datta, K. K. R.; Ji, Q.; Hill, J. P.; Abe, H.; Honma, I.; Ariga, K. Open-Mouthed Metallic Microcapsules: Exploring Performance Improvements at Agglomeration-Free Interiors. *Journal of the American Chemical Society* **2010,** *132* (41), 14415.

(24) Landon, P. B.; Mo, A. H.; Zhang, C.; Emerson, C. D.; Printz, A. D.; Gomez, A. F.; DeLaTorre, C. J.; Colburn, D. A. M.; Anzenberg, P.; Eliceiri, M.et al. Designing Hollow Nano Gold Golf Balls. *ACS Applied Materials & Interfaces* **2014,** *6* (13), 9937.

(25) Wang, S.; Chen, M.; Wu, L. One-Step Synthesis of Cagelike Hollow Silica Spheres with Large Through-Holes for Macromolecule Delivery. *ACS Applied Materials & Interfaces* **2016,** *8* (48), 33316.

(26) Wu, S.-H.; Mou, C.-Y.; Lin, H.-P. Synthesis of mesoporous silica nanoparticles. *Chemical Society Reviews* **2013,** *42* (9), 3862.

(27) Deng, Y.; Wei, J.; Sun, Z.; Zhao, D. Large-pore ordered mesoporous materials templated from non-Pluronic amphiphilic block copolymers. *Chemical Society Reviews* **2013,** *42* (9), 4054.

(28) Junhao, M.; Yuan, R.; Xinran, Z.; Liangliang, L.; Yongheng, Z.; Xiaowei, C.; Pengcheng, X.; Xinxin, L.; Yonghui, D.; Dongyuan, Z. Sensors: Pt Nanoparticles Sensitized Ordered Mesoporous WO3 Semiconductor: Gas Sensing Performance and Mechanism Study (Adv. Funct. Mater. 6/2018). *Advanced Functional Materials* **2018,** *28* (6), 1870040.

(29) Wan, Y.; Zhao. On the Controllable Soft-Templating Approach to Mesoporous Silicates. *Chemical Reviews* **2007,** *107* (7), 2821.

(30) Zhu, Y.; Zhao, Y.; Ma, J.; Cheng, X.; Xie, J.; Xu, P.; Liu, H.; Liu, H.; Zhang, H.; Wu, M.et al. Mesoporous Tungsten Oxides with Crystalline Framework for Highly Sensitive and Selective Detection of Foodborne Pathogens. *Journal of the American Chemical Society* **2017,** *139* (30), 10365.

(31) Begum, G.; Rana, R. K. Bio-inspired motifs via tandem assembly of polypeptides for mineralization of stable CaCO3 structures. *Chemical Communications* **2012,** *48* (66), 8216.

(32) Liu, Y.; Cui, Y.; Guo, R. Amphiphilic Phosphoprotein-Controlled Formation of Amorphous Calcium Carbonate with Hierarchical Superstructure. *Langmuir* **2012,** *28* (14), 6097.

(33) Lu, Y.; Cai, C.; Lin, J.; Zhuang, Q. Formation of CaCO3 fibres directed by polypeptide vesicles. *Journal of Materials Chemistry B* **2016,** *4* (21), 3721.

(34) Schulz, A.; Liebeck, B. M.; John, D.; Heiss, A.; Subkowski, T.; Boker, A. Protein-mineral hybrid capsules from emulsions stabilized with an amphiphilic protein. *Journal of Materials Chemistry* **2011,** *21* (26), 9731.

(35) Khanal, A.; Inoue, Y.; Yada, M.; Nakashima, K. Synthesis of Silica Hollow Nanoparticles Templated by Polymeric Micelle with Core−Shell−Corona Structure. *Journal of the American Chemical Society* **2007,** *129* (6), 1534.

(36) Liu, D., Ph. D. dissertation, 2009.

(37) Liu, D.; Sasidharan, M.; Nakashima, K. Micelles of poly(styrene-b-2-vinylpyridine-b-ethylene oxide) with blended polystyrene core and their application to the synthesis of hollow silica nanospheres. *Journal of Colloid and Interface Science* **2011,** *358* (2), 354.

(38) Bastakoti, B. P.; Guragain, S.; Yokoyama, Y.; Yusa, S.-i.; Nakashima, K. Synthesis of Hollow CaCO3 Nanospheres Templated by Micelles of Poly(styrene-b-acrylic acid-b-ethylene glycol) in Aqueous Solutions. *Langmuir* **2010,** *27* (1), 379.

(39) ALOthman, Z. A review: Fundamental aspects of silicate mesoporous materials. *Materials* **2012,** *5* (12), 2874.

(40) Liu, J.; Bai, S.; Zhong, H.; Li, C.; Yang, Q. Tunable Assembly of Organosilica Hollow Nanospheres. *The Journal of Physical Chemistry C* **2009,** *114* (2), 953.

(41) Gohy, J. F.; Willet, N.; Varshney, S.; Zhang, J. X. a.; Jérôme, R. pH Dependence of the morphology of aqueous micelles formed by polystyrene-block-poly(2-vinylpyridine)-block-poly(ethylene oxide) copolymers *e-Polymer* **2002**, 35.

(42) Alam, M. M.; Yamahana, H.; Bastakoti, B. P.; Luitel, H. N.; Zhao, W.; Yamauchi, Y.; Watari, T.; Noguchi, H.; Nakashima, K. Synthesis of hollow silica nanosphere with high accessible surface area and their hybridization with carbon matrix for drastic enhancement of electrochemical property. *Applied Surface Science* **2014,** *314*, 552.

(43) Pucić, I.; Jurkin, T. FTIR assessment of poly(ethylene oxide) irradiated in solid state, melt and aqeuous solution. *Radiation Physics and Chemistry* **2012,** *81* (9), 1426.

(44) Sasidharan, M.; Liu, D.; Gunawardhana, N.; Yoshio, M.; Nakashima, K. Synthesis, characterization and application for lithium-ion rechargeable batteries of hollow silica nanospheres. *Journal of Materials Chemistry* **2011,** *21* (36), 13881.

(45) Mochane, M. J.; Luyt, A. S. Preparation and properties of polystyrene encapsulated paraffin wax as possible phase change material in a polypropylene matrix. *Thermochimica Acta* **2012,** *544*, 63.

(46) Borodina, T.; Grigoriev, D.; Mohwald, H.; Shchukin, D. Hydrogen storage materials protected by a polymer shell. *Journal of Materials Chemistry* **2010,** *20* (8), 1452.

(47) http://orgchemboulder.com/Spectroscopy/irtutor/aromaticsir.shtml. (accessed on 15 July 2017).

(48) Karayianni, M.; Pispas, S. In *Fluorescence Studies of Polymer Containing Systems*; Procházka, K., Ed.; Springer International Publishing: Cham, 2016, DOI:10.1007/978-3-319-26788-3_2 10.1007/978-3-319-26788-3_2.

(49) Kostiv, U.; Janouskova, O.; Slouf, M.; Kotov, N.; Engstova, H.; Smolkova, K.; Jezek, P.; Horak, D. Silica-modified monodisperse hexagonal lanthanide nanocrystals: synthesis and biological properties. *Nanoscale* **2015,** *7* (43), 18096.

(50) Huang, Z.; Wu, P.; Gong, B.; Dai, Y.; Chiang, P.-C.; Lai, X.; Yu, G. Efficient Removal of Co 2+ from Aqueous Solution by 3-Aminopropyltriethoxysilane Functionalized Montmorillonite with Enhanced Adsorption Capacity. *PloS One* **2016,** *11* (7), e0159802.

(51) Yang, J.; Hu, D.; Fang, Y.; Bai, C.; Wang, H. Novel Method for Preparation of Structural Microspheres Poly(N-isopropylacrylamide-co-acrylic acid)/SiO2. *Chemistry of Materials* **2006,** *18* (20), 4902.

(52) Neville, F.; Seyfaee, A. Real-Time Monitoring of in Situ Polyethyleneimine-Silica Particle Formation. *Langmuir* **2013,** *29* (47), 14681.

(53) Fu, X.; He, X.; Hu, X. Preparation of single-hole silica hollow microspheres by precipitation-phase separation method. *Colloids and Surfaces A: Physicochemical and Engineering Aspects* **2012,** *396*, 283.

(54) Guignard, F.; Lattuada, M. Template-Assisted Synthesis of Janus Silica Nanobowls. *Langmuir* **2015,** *31* (16), 4635.

(55) G., G.; Z., Z.; Z., W.; B., L.; D., G.; C., X. Single-Hole Hollow Polymer Microspheres toward Specific High-Capacity Uptake of Target Species. *Advanced Materials* **2007,** *19* (17), 2370.

(56) Jeong, U.; Im, S. H.; Camargo, P. H. C.; Kim, J. H.; Xia, Y. Microscale Fish Bowls: A New Class of Latex Particles with Hollow Interiors and Engineered Porous Structures in Their Surfaces. *Langmuir* **2007,** *23* (22), 10968.

(57) Leung, K.; Nielsen, I. M. B.; Criscenti, L. J. Elucidating the Bimodal Acid−Base Behavior of the Water−Silica Interface from First Principles. *Journal of the American Chemical Society* **2009,** *131* (51), 18358.

(58) Brinker, C. J.; Scherer, G. W. *Sol-gel science: the physics and chemistry of sol-gel processing*; Academic Press, 2013.

(59) Hench, L. L.; West, J. K. The sol-gel process. *Chemical reviews* **1990,** *90* (1), 33.

(60) Hotta, Y.; Alberius, P. C. A.; Bergstrom, L. Coated polystyrene particles as templates for ordered macroporous silica structures with controlled wall thickness. *Journal of Materials Chemistry* **2003,** *13* (3), 496.

(61) van Bommel, K. J. C.; Shinkai, S. Silica Transcription in the Absence of a Solution Catalyst: The Surface Mechanism. *Langmuir* **2002,** *18* (12), 4544.

(62) Zhao, D.; Feng, J.; Huo, Q.; Melosh, N.; Fredrickson, G. H.; Chmelka, B. F.; Stucky, G. D. Triblock Copolymer Syntheses of Mesoporous Silica with Periodic 50 to 300 Angstrom Pores. *Science* **1998,** *279* (5350), 548.

(63) Zhang, G.; Yu, Y.; Chen, X.; Han, Y.; Di, Y.; Yang, B.; Xiao, F.; Shen, J. Silica nanobottles templated from functional polymer spheres. *Journal of Colloid and Interface Science* **2003,** *263* (2), 467.

(64) Yi, D.; Zhang, Q.; Liu, Y.; Song, J.; Tang, Y.; Caruso, F.; Wang, Y. Synthesis of Chemically Asymmetric Silica Nanobottles and Their Application for Cargo Loading and as Nanoreactors and Nanomotors. *Angewandte Chemie International Edition* **2016,** *55* (47), 14733.

(65) Wang, S.; Zhang, M.; Wang, D.; Zhang, W.; Liu, S. Synthesis of hollow mesoporous silica microspheres through surface sol–gel process on polystyrene-co-poly(4-vinylpyridine) core–shell microspheres. *Microporous and Mesoporous Materials* **2011,** *139* (1–3), 1.

(66) Liu, T.; Xu, G.; Gong, H.; Pang, J.; He, F. Effect of Alcohols on Aggregation Behaviors of Branched Block Polyether Tetronic 1107 at an Air/Liquid Surface. *Langmuir* **2011,** *27* (15), 9253.

(67) Chaibundit, C.; Ricardo, N. M. P. S.; Ricardo, N. M. P. S.; Costa, F. d. M. L. L.; Wong, M. G. P.; Hermida-Merino, D.; Rodriguez-Perez, J.; Hamley, I. W.; Yeates, S. G.; Booth, C. Effect of Ethanol on the Micellization and Gelation of Pluronic P123. *Langmuir* **2008,** *24* (21), 12260.

(68) De, G.; Karmakar, B.; Ganguli, D. Hydrolysis-condensation reactions of TEOS in the presence of acetic acid leading to the generation of glass-like silica microspheres in solution at room temperature. *Journal of Materials Chemistry* **2000,** *10* (10), 2289.

(69) Cai, Y.; Xie, H.; Sun, J.; Liu, H.; Wang, J.; Zhou, Y.; Nie, W.; Song, L. Weak acid–base interaction induced assembly for the formation of berry-like polystyrene/SiO2 composite particles. *Materials Chemistry and Physics* **2013,** *137* (3), 796.

866

867

868

869

870

871

872

873

874

875

876 **TABLE OF CONTENTS/ABSTRACT GRAPHIC**

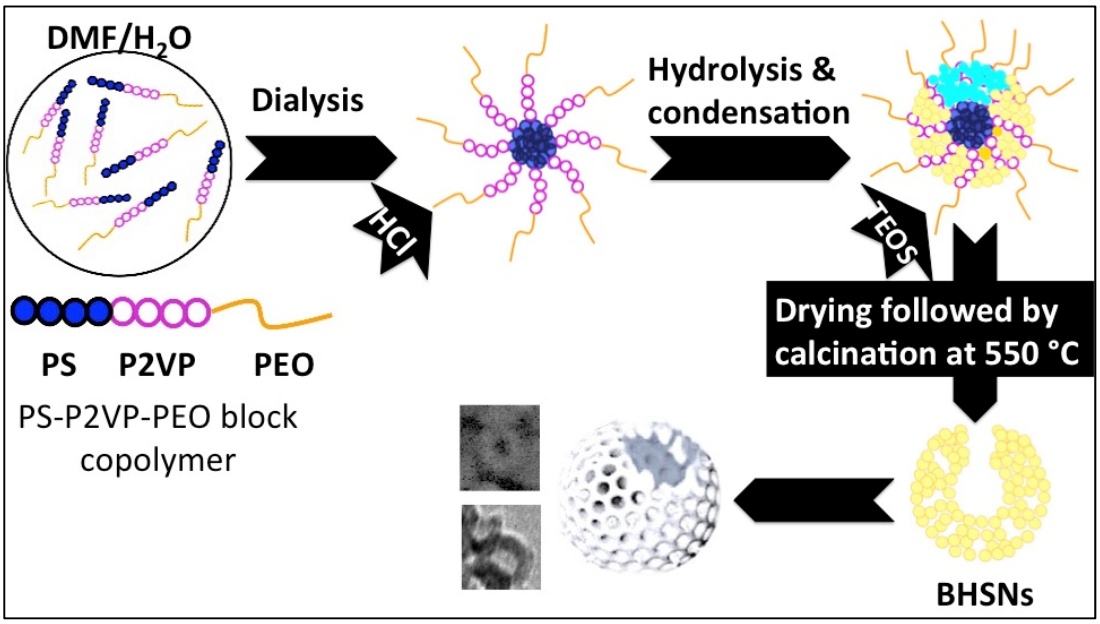
DMF/H2O
Dialysis
HCl
Hydrolysis &
condensation
TEOS
Drying followed by
calcination at 550 °C
PS
P2VP
PEO
PS-P2VP-PEO block
copolymer
BHSNs

877